Optics & Laser Technology 164 (2023) 109471

Contents lists available at ScienceDirect

Optics and Laser Technology

journal homepage: www.elsevier.com/locate/optlastec

Full length article

Dynamic control of multi-channel plasmonic vector vortex with integer- and fractional-order based on mode extraction

Yu Miao [a], Xiaoyu Weng [b,c,*], Mingzhu Xu [a], Jun He [d], Liwei Liu [b,c], Changrui Liao [d], Yiping Wang [d], Xiumin Gao [a,*], Baolin Liu [a], Junle Qu [b,c], Songlin Zhuang [a]

[a] Engineering Research Center of Optical Instrument and System, Ministry of Education, Shanghai Key Lab of Modern Optical System, School of Optical-Electrical and Computer Engineering, University of Shanghai for Science and Technology, 516 Jungong Road, Shanghai 200093, China
[b] State Key Laboratory of Radio Frequency Heterogeneous Integration, Shenzhen University, Shenzhen 518060, China
[c] College of Physics and Optoelectronic Engineering, Key Laboratory of Optoelectronic Devices and Systems of Ministry of Education and Guangdong Province, Shenzhen University, Shenzhen 518060, China
[d] Shenzhen Key Laboratory of Photonic Devices and Sensing Systems for Internet of Things, Guangdong and Hong Kong Joint Research Centre for Optical Fibre Sensors, Shenzhen University, Shenzhen 518060, China

ARTICLE INFO

Keywords:
Plasmonic vector vortex
The principle of mode extraction
Optical pen

ABSTRACT

Plasmonic vector vortex created by coupling vector vortex beam to microstructure on metal dielectric interface has attracted great interests in the research field of nanophotonics. However, the complicated polarization of incident vector beam and the excitation way of plasmonic waves based on the fixed microstructure give rise to big challenges in controlling plasmonic vector vortex mode with arbitrary order in a real-time and dynamically. Here, we solve this scientific problem by generating multi-channel plasmonic vector vortex with integer- and fractional-order using the principle of mode extraction along with optical pen. Without changing the polarization state of incident vector beam, plasmonic vector vortex mode in each channel is extracted directly from a high-order vector vortex beam based on the principle of mode extraction. The number, position, amplitude and phase of plasmonic vector vortex mode can further be arranged in an arbitrary manner with the aid of optical pen on the gold film. This work presents a flexible method of tailoring complicated plasmonic field on a metal film, which may offer new possibilities for the applications of plasmonic tweezers, Raman imaging etc.

1. Introduction

Vortex is an intrinsic morphological feature of waves that exists widely in nature. In classical optics, vector vortex beam (VVB) is the vectorial form of optics vortex, which can be considered as the superposition of two left and right circularly polarized beams with inverse optical vortices [1]. A polarization singularity is therefore formed in the center of VVB. Normally, there are two kinds of propagable VVBs; one is m-order VVB; another is $m + 0.5$-order VVB with ± 0.5 topological charge [1,2]. Here, the orders m, $m + 0.5$ relate to the inherent topological charge of both circular polarized beams, and m is an integer. Although VVB is created by two vortex beams, the unique polarization state of VVB gives rise to peculiar properties [3,4], thereby motivating a wide-range of applications in optics, including vectorial Doppler effect [5], optical communication [6], advanced lasers [7].

Besides the above interesting researches, plasmonic vector vortex (PVV) induced by a m-order VVB on the surface of metal film has also attracted great interests in recent decades [8–10]. Because of the dominant longitude component of surface plasmon polariton (SPP) field, PVV provides new possibilities in the field of nanophotonics, thereby giving rise to wide-range of applications, including particle manipulation [11–13], optical imaging [14–16], sensors [17] and plasmonic surface-enhanced Raman scattering [18]. For example, massive energy densities can be achieved by the plasma resonance between metal film and metal particle when focusing 0- and 1-order VVB, namely radially and linearly polarized beam [13,19,20]. Strong optical force can therefore be obtained, which is demonstrated to be a powerful tool to trap metal particle [11,12] and rotate metal nanorod [13]. Moreover, taking advantage of these massive energy densities, Raman signal can also be enhanced in the application of plasmonic surface-enhanced Raman scattering [18] and Raman imaging [15,16]. Besides being of applied interests in optics, PVV plays a vital role on many attractive

* Corresponding authors.
E-mail addresses: xiaoyu@szu.edu.cn (X. Weng), gxm@usst.edu.cn (X. Gao).

https://doi.org/10.1016/j.optlastec.2023.109471
Received 30 January 2023; Received in revised form 28 March 2023; Accepted 4 April 2023
Available online 11 April 2023

fundamental researches as well, including optical spin-to-orbital plasmonic angular momentum conversion [20,21], optical transverse spin [22], photonic skyrmions [23].

Despite these valuable researches, PVV cannot be manipulated easily like its scalar counterpart, namely plasmonic vortex [23]. As a scalar vortex on the surface of metal film, plasmonic vortex with arbitrary topological charge can simply be achieved using a well-designed metasurface [24,25], a ring coupler [26,27], and a high numerical aperture (NA) focusing configuration [28]. However, unlike plasmonic vortex, PVV is related to the polarization of incident vector beam instead of its scalar vortex phase. That is, once the order of incident VVB is determined, PVV coupling on the metal film cannot be adjusted any more [10]. For this reason, one can only obtain a particular order of PVV mode at a time. For example, PVV array with order 1 can be created using a Dammann grating along with an incident 1-order VVB [29,30]. Although the topological charge of each PVV can be adjusted at will by the parameter of Dammann grating, the polarization mode of each PVV is merely determined by the incident 1-order VVB, thereby possessing only an identical PVV mode with the order 1 in the array [30]. Is it possible to create multiple PVV channels, where each channel can be adjusted individually? If so, one can achieve multiple PVV modes with not only tunable topological charge, but also, more importantly, adjustable order. However, to the best of our knowledge, such multi-channel PVV modes have not been realized so far.

In this paper, we solve this scientific problem by creating multi-channel PVV with integer- and fractional-order using the principle of mode extraction along with optical pen. When focusing an incident VVB in a high-NA focusing system, ring-shape SPPs can be induced on the surface of gold film, thereby interfering together to form a PVV mode in the center of excitation ring. Because the ring-shape SPPs are induced by the incident VVB, the phase of SPPs has a one-to-one correspondence with that of incident VVB. By merely adjusting the phase of incident high-order VVB, one can not only extract PVV with arbitrary order in each channel (different polarization mode) directly and individually using the principle of mode extraction, but also control the number, position, amplitude and vortex phase of PVV at will using the optical pen [31]. This work demonstrates the dynamic control of multi-channel PVV with different order and vortex phase, which may offer promising applications in many scientific studies, such as optical imaging [14–16], dynamic plasmonic tweezers [11,13], etc.

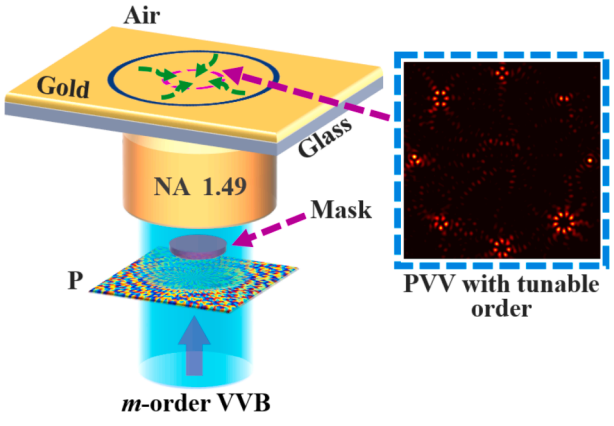

Fig. 1. Schematic of SPPs excitation system. An incident *m*-order VVB modulated by the pupil filter P and a Mask is focused by an oil immersion lens. The focusing *m*-order VVB can therefore be coupled into ring-shape SPPs (green arrows) on the gold film, which further interfere with each other to form multi-channel PVV modes in the center of the excitation ring. (For interpretation of the references to colour in this figure legend, the reader is referred to the web version of this article.)

2. Theoretical model

Fig. 1 shows the schematic of dynamically controlling multi-channel PVV with integer- and fractional-order. Here, the entire SPPs excitation system is composed of a three-layer structure system and a high-NA focusing system. For the former one, the three-layer structure system consists of a gold film sandwiched between air and glass substrate. For the latter one, an oil immersion lens in the high-NA focusing system is utilized to couple incident VVB into ring-shape SPPs so that the wavevector of the incident light beam matches with that of SPPs on the gold film. In this case, the refractive index of the immersion oil is equal to that of the glass substrate.

2.1. Excitation of SPPs using a m-order VVB

In the first process, a collimated incident *m*-order VVB modulated by a pupil filter (P) and a mask is focused by an oil immersion lens in Fig. 1. When the focused VVB passes through the three-layer system, most of the light beams are reflected by the gold film, and only two kinds of light beams are retained on the gold film. One is the transmission light beam; another is the ring-shape SPPs, which are induced by the incident VVB within the resonance angle of glass- gold-air system. Here, pure SPPs can easily be obtained on the gold film by eliminating the transmission light beam using a mask in Fig. 1. According to the Fresnel formula, *p*- and *s*-components of incident vector beam possess different transmittances when passing through the three-layer system. Thus, ring-shape SPPs can be expressed as [2,30]

$$\mathbf{E}_{VVBs} = T_p T_m \left[t_p \cos(m-1)\varphi \mathbf{e}_r + t_s \sin(m-1)\varphi \mathbf{e}_\varphi \right] \tag{1}$$

Here, T_p denotes the transmission of pupil filter P, which is derived in Section 2.3. T_m is the transmittance of the mask before the oil immersion lens. m is the order of incident VVB. φ represents the azimuthal angle.$\mathbf{e}_r$ and $\mathbf{e}_\varphi$ are the unit vectors in the radial and azimuthal directions, and can be expressed as [3]

$$\mathbf{e}_r = \cos\varphi \mathbf{e}_x + \sin\varphi \mathbf{e}_y \tag{2}$$

$$\mathbf{e}_\varphi = -\sin\varphi \mathbf{e}_x + \cos\varphi \mathbf{e}_y \tag{3}$$

respectively.$\mathbf{e}_x$ and $\mathbf{e}_y$ are the unit vectors in the x and y directions, respectively.

In Eq. (1), t_p and t_s are the transmittances of the *p*- and *s*-components, respectively, which can be calculated as

$$t_p = \frac{t_{p12} t_{p23} \exp(ik_{2z}d)}{1 + r_{p12} r_{p23} \exp(i2k_{2z}d)} \tag{4}$$

$$t_s = \frac{t_{s12} t_{s23} \exp(ik_{2z}d)}{1 + r_{s12} r_{s23} \exp(i2k_{2z}d)} \tag{5}$$

where t_{pij} and t_{sij} are the Fresnel transmittance coefficients for the *p*- and *s*-components at the i/j interface. r_{pij} and r_{sij} are their counterpart reflection coefficients. $i, j = 1, 2, 3$ denote the glass, gold film and air in Fig. 1, respectively. d and k_{2z} are the thickness of gold film and the *z*-component wavevector on the gold film, respectively.

2.2. Intensity of Multi-channel PVV

In the second process, ring-shape SPPs in Eq. (1) is created by the incident *m*-order VVB within the resonance angle of glass-gold-air system. As shown in Fig. 1, ring-shape SPPs indicated by the green arrow are further propagating toward the center of SPPs ring, thereby interfering together to form multi-channel PVV on the gold film. Mathematically, based on the Debye vectorial diffraction theory, the electric field in the center of SPPs ring can be expressed as [3]

$$\mathbf{E} = \frac{-iA}{\pi}\int_0^{\alpha}\int_0^{2\pi}\sin\theta\sqrt{\cos\theta}T_p T_m l_0(\theta)\mathbf{V}\exp(-ikn_3\mathbf{s}\bullet\rho)d\varphi d\theta \tag{6}$$

where A is a normalized constant; θ is the convergent angle; $\alpha = \arcsin(NA/n_1)$ represents the maximum convergent angle of θ. NA is the numerical aperture of oil immersion lens. n_1, n_2, n_3 are the refractive indexes of glass, metal and air in the focusing space, respectively. The incident wavenumber $k = 2\pi/\lambda$, and λ is the wavelength of the incident m-order VVB. $\rho = (r\cos\phi, r\sin\phi, z)$ denotes the position vector of an arbitrary point (r, ϕ, z) in the focal region. The unit vector $\mathbf{s} = (-\sin\theta_3\cos\varphi, -\sin\theta_3\sin\varphi, \cos\theta_3)$ implies the direction of wavevector, where

$$\theta_3 = \arcsin\left(\frac{n_1}{n_3}\sin\theta\right) \tag{7}$$

$l_0(\theta)$ denotes the electric amplitude of the incident m-order VVB, which can be expressed as [32]

$$l_0(\theta) = J_1(2\beta_0\sin\theta/\sin\alpha)\exp[-(\beta_0\sin\theta/\sin\alpha)^2] \tag{8}$$

Here, the ratio of the pupil radius to the incident beam waist $\beta_0 = 1.5$ in this paper. $J_1(\bullet)$ is the Bessel function of the first kind with order 1.

The transmittance of the mask before the oil immersion lens can be expressed as

$$T_m = \begin{cases} 0 & 0\leqslant\theta\leqslant\beta \\ 1 & \beta\leqslant\theta\leqslant\alpha \end{cases} \tag{9}$$

where the blocking angle of the mask β is determined by the excitation angle of SPPs.

In Eq. (6), $\mathbf{V}$ represents the propagation unit vector of the incident m-order VVB right after having passed through oil immersion lens. According to the electric field of ring-shape SPPs in Eq. (1), $\mathbf{V}$ can be written as [2,32]

$$\mathbf{V} = \cos(m-1)\varphi\mathbf{V}_r + \sin(m-1)\varphi\mathbf{V}_\varphi \tag{10}$$

where $\mathbf{V}_r$ and $\mathbf{V}_\varphi$ are the electric vectors of $\mathbf{e}_r$ and $\mathbf{e}_\varphi$, respectively, and can be written as

$$\mathbf{V}_r = \begin{bmatrix} t_p^r\cos\theta\cos(\varphi-\phi) & t_p^r\cos\theta\sin(\varphi-\phi) & t_p^z\sin\theta \end{bmatrix}^T \tag{11}$$

$$\mathbf{V}_\varphi = t_s\begin{bmatrix} -\sin(\varphi-\phi) & \cos(\varphi-\phi) & 0 \end{bmatrix}^T \tag{12}$$

Here, the transmittance coefficients for the p- and z-components in the focal region $t_p^r = \tau_r t_p$, $t_p^z = \tau_z t_p$, respectively, where $\tau_r = \sqrt{n_3^2 - n_1^2\sin^2\theta}/n_3^2\cos\theta$ and $\tau_z = n_1/n_3$.

Eventually, the intensity of multi-channel PVV with integer- and fractional-order can be obtained using $I = |\mathbf{E}|^2$.

2.3. Derivation of pupil filter P in Eq. (6)

In classical optics, l- and $l+0.5$ order VVB are two propagable VVBs, which can be expressed as [2]

$$\mathbf{E}_{integer} = \begin{bmatrix} \cos(l\varphi+\varphi_0) \\ \sin(l\varphi+\varphi_0) \end{bmatrix} \tag{13}$$

$$\mathbf{E}_{fractional} = \exp(\pm 0.5i\varphi)\begin{bmatrix} \cos[(l+0.5)\varphi+\varphi_0] \\ \sin[(l+0.5)\varphi+\varphi_0] \end{bmatrix} \tag{14}$$

Here, φ_0 is an angle that rotates the polarization state of entire l- and $l+0.5$ order VVB. For example, radially polarized beam can be obtained with $l = 1$ and $\varphi_0 = 0$, while its orthogonal counterpart, namely azimuthally polarized beam, is achieved with $l = 1$ and $\varphi_0 = 0.5\pi$.

As mentioned above, multi-channel PVV with tunable integer- and fractional-order is created using only a single light beam, namely m-order VVB. This physical process involves two important principles in optics, namely the principle of mode extraction [32] and the optical pen [31], respectively. For the former one, mode extraction conveys an important physical idea that arbitrary polarization modes can be extracted directly from a single vector beam. Based on this principle, PVVs with integer- and fractional-order link to different symmetrical petal-like phases in Fig. 2. Specifically, the petal number for integer-order PVV is $2|m-l|$, while that of fractional-order PVV is $2|m-l+0.5|$. Here, $l = 0, \pm1, \pm2...$ In this case, the phase for PVV with integer- and fractional-order can be expressed as [2,32]

$$\phi_i = Phase\{\cos[(m-l)\varphi+\varphi_0]\} \tag{15}$$

$$\phi_f = Phase\{\cos[(m-l+0.5)\varphi+\varphi_0]\} \pm 0.5\varphi \tag{16}$$

respectively.

As shown in Fig. 2, mode extraction is responsible for the control of PVV mode, while the channel information, such as amplitude, phase, number and position, are adjusted by the optical pen. As demonstrated in Ref [31], optical pen is developed based on the compensation of optical path difference, which can be expressed as

$$\psi_o = Phase\left\{\sum_{j=1}^{N} PF(s_i, x_j, y_j, z_j, \delta_j)\right\} \tag{17}$$

Here, x_j, y_j, z_j indicates the positions of the j-th channel of PVV on the gold film. s_j and δ_j control its amplitude and phase, respectively. N is the number of multi-channel of PVV.

Finally, the overall phase of pupil filter P for multi-channel PVV can simply be obtained by $\Omega_p = \phi_{if} + \psi_o$. That is, the transmission of pupil filter P can be simplified to

$$T_p = \exp(i\Omega_p) \tag{18}$$

3. Results and analyses

3.1. Transmittance of the mask

Fig. 3 shows the Dependence of Fresnel coefficient upon the convergent angle θ for the p-, z- and s-components $|t_p^r|^2$, $|t_p^z|^2$, $|t_s|^2$. Here, the wavelength of incident m-order VVB $\lambda = 532$ nm and the thickness of gold film $d = 50$ nm. The numerical aperture of oil immersion lens $NA = 1.49$. The refractive indices of glass, gold and air $n_1 = 1.518$, $n_2 =$

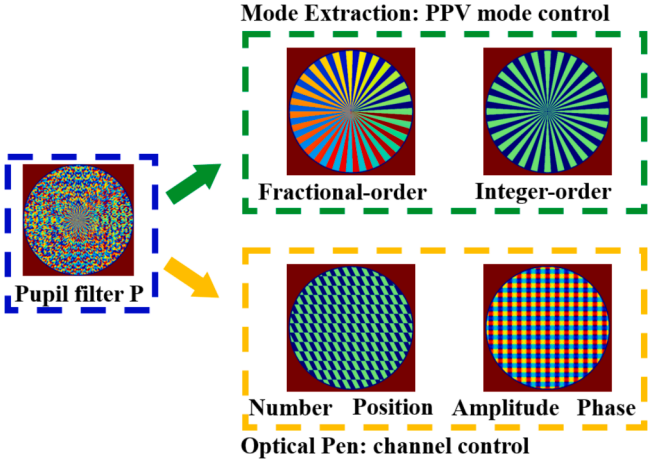

Fig. 2. Optical information of pupil filter P. Pupil filter P in Fig. 1 contains two important information in optics: one is the principle of mode extraction, which is responsible for switching PVV mode with integer- and fractional-order; another is the optical pen, which can adjust the number, position, amplitude and phase of PVV modes on the gold film.

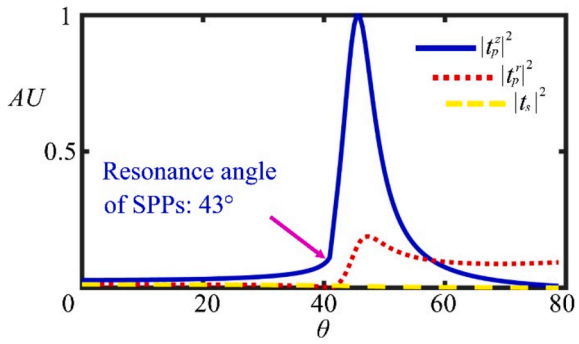

Fig. 3. Dependence of Fresnel coefficient upon the convergent angle θ. Here, the blue solid line, red dot line and yellow dash line present $|t_p^r|^2$, $|t_p^z|^2$, $|t_s|^2$, respectively. (For interpretation of the references to colour in this figure legend, the reader is referred to the web version of this article.)

$0.54386 + 2.2309i$, and $n_3 = 1$, respectively. In principle, the s-component of incident VVB cannot excite SPPs on the gold film. Therefore, both p-, z- components of SPPs in Fig. 3 come from the p-component of incident VVB in Eq. (1). The relationship $\tau_z > \tau_r$ implies that PVV created on the gold film is dominated by the z- components of SPPs. In addition, according to t_p in Eq. (4), both p-, z- components possess an identical resonance angle with about $40^0 < \theta < 60^0$. For this reason, to eliminate the transmission light beam on the gold film, the blocking angle of the mask $\beta = 40^0$ in Eq. (9). In the following simulations, we take the incident $m = 30$-order VVB as an example to extract multi-channel PVV on the gold film in Fig. 1. Note that the unit of length in all figures is the wavelength λ and the intensities of PVV are normalized to be a unit value.

3.2. Switching PVV mode using mode extraction

Fig. 4 presents an example of switching PVV mode at will on the gold film. PVVs with the order of −0.5, −2.5, 3 and 6 in Fig. 4 (b, g, l, q) are induced by a $m = 30$-order VVB with the phases in Fig. 4 (a, f, k, p), respectively. Fig. 4 (c, h, m, r) and (d, i, n, s) are their corresponding longitudinal and transverse components. The polarization of inherent modes within the incident $m = 30$-order VVB that correspond with PVVs in Fig. 4 (b, g, l, q) are shown in Fig. 4 (e, j, o, t), respectively, and can be expressed as in Equations (13, 14) with $\varphi_0 = 0$. According to the principle of mode extraction, different kind of phase links to different order VVB, thereby inducing PVV mode with integer- and fractional-order on the gold film. Specifically, in term of integer-order PVV mode, one can link the phase ϕ_i in Eq. (15) with the inherent polarization mode within the incident vector beam, namely l-order VVB mode. In this case, PVV modes with the order $l = 3, 6$ in Fig. 4 (l, q) can be obtained on the gold film using the phases in Fig. 4 (k, p). In term of fractional-order PVV mode, the inherent polarization mode of $l + 0.5$-order VVB can be achieved by the phase ϕ_i with $l = l + 0.5$ in Eq. (15) as well. However, due to the polarization discontinuousness along the x axis, see Fig. 4 (e, j), $l + 0.5$-order VVB cannot maintain in free space. For this reason, PVV with $l + 0.5$-order cannot be created on the gold film. To maintain the polarization of $l + 0.5$-order VVB in free space, the polarization discontinuousness along the x axis must be compensated by the phase jump of vortex phase $\pm 0.5\varphi$ in Eq. (16). In this way, the phase ϕ_f in Eq. (16) is also symmetrical like that of integer order VVB in Eq. (15), as shown in Fig. 4 (a, f, k, p). That is, one can simply obtain PVV modes with the order $l + 0.5$ using the phase ϕ_f in Eq. (16). Here, the petal number $2|M|$ in Fig. 4 implies the order of PVV, where $M = l$ for integer-order PVV and $M = l + 0.5$ for fractional-order PVV. From above, the polarization mode of PVV is merely controlled by the phase of incident $m = 30$-order VVB. That is, without having to change the incident $m = 30$-order VVB, one can switch the order of PVV dynamically by merely adjusting its phase.

Fig. 4 not only verifies that PVV can be switched at will by a particular phase, but also opens new ways to control the channel information of PVV with the aid of optical pen. Taking 2-order PVV as an example. As shown in Fig. 5, one can simply create a 2-order PVV mode on the gold film by extracting the 2-order VVB mode from the incident $m = 30$-order VVB using the phase in Eq. (15) with $l = 2$. The mode of 2-order PVV can be tuned freely by the parameter φ_0, where $\varphi_0 = 0, 0.25\pi$,

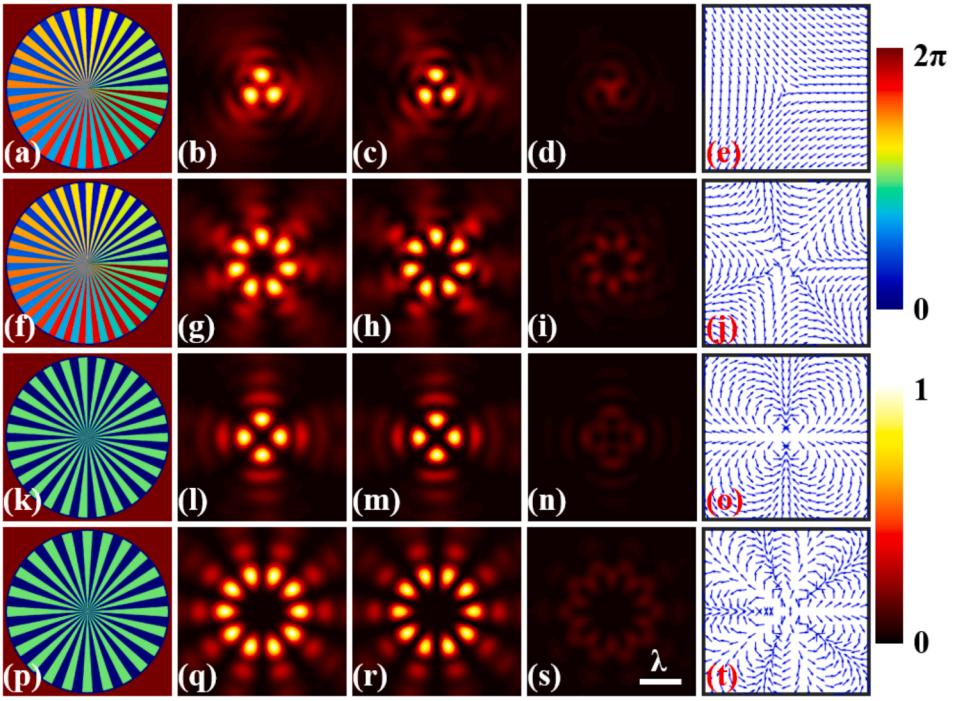

Fig. 4. Switching PVV with integer- and fractional-order using mode extraction. PVVs with the order of −0.5 (b), −2.5 (g), 3 (l) and 6 (q) are extracted from a $m = 30$-order VVB by the phases in (a, f, k, p), respectively. Subfigures (c, h, m, r) and (d, i, n, s) are their corresponding longitudinal and transverse components. The polarizations of inherent modes within $m = 30$-order VVB that correspond with PVVs in (b, g, l, q) are shown in (e, j, o, t), respectively.

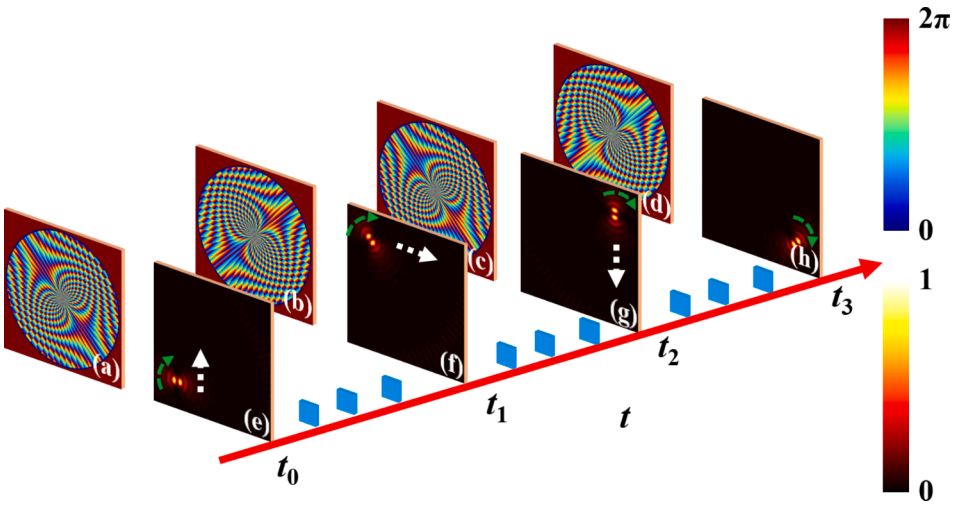

Fig. 5. Control of PVV channel using optical pen. With the aid of optical pen, PVV channel can be manipulated in a real-time and dynamically. Here, 2-order PVV moves from the start point in (-3, −3) to the final point in (3, −3) on the gold film by changing the phase from (a) to (d). The white and green arrow imply the trajectory of PVV and the polarization state of 2-order PVV with φ_0, respectively. Here, (a, e) $\varphi_0 = 0$; (b, f) $\varphi_0 = 0.25\pi$; (c, g) $\varphi_0 = 0.5\pi$; (d, h) $\varphi_0 = 0.75\pi$. (For interpretation of the references to colour in this figure legend, the reader is referred to the web version of this article.)

0.5π, 0.75π for Fig. 5 (e, f, g, h), respectively. Therefore, the petal-like intensity of PVV mode in Fig. 5 is rotating along with the parameter φ_0, which is indicated by the green arrow. Beside the adjustment of PVV mode, its trajectory can also be controlled by the optical pen. Specifically, as shown in Fig. 5, PVV with the order of 2 can not only rotate with the parameter φ_0, but also move from the start point in (-3, −3) to the final point in (3, −3) on the gold film by changing the phase from Fig. 5 (a) to Fig. 5 (d). The white arrow implies the trajectory of PVV. Generally, the phase of a light beam can be adjusted in a real-time and dynamically by a phase-only spatial light modulator (SLM). For this reason, as time goes by, one can achieve tunable polarization mode of PVV with arbitrary moving trajectory on the gold film.

3.3. Creation of multi-channel PVV modes

As shown in Fig. 2, pupil filter P contains two critical information of manipulating PVV modes. One is the mode extraction, which is the fundamental principle for the switch of PVV mode; another is the optical pen, which is responsible for the channel control of PVV modes. Therefore, we can not only switch a single PVV modes at will, but also create multi-channel PVV modes on the gold film. By comparing with that of plasmonic focus array in Ref [29,30], we firstly create 1-order PVV mode with 3 × 3 channels in Fig. 6(f). Here, Fig. 6 (k) shows their topological charges. The polarization mode of PVV in each channel possess an identical polarization property like that created by a radially polarized beam with a Dammann grating [29,30]. Note that Dammann grating is a special solution of optical pen [31]. Therefore, the phase of incident m = 30-order VVB in Fig. 1 can be considered as the superposition of ϕ_i and a Dammann grating, see Fig. 6(a). By adjusting the parameter of Dammann grating realized by optical pen, the topological charge of each 1-order PVV mode can be altered symmetrically like that of Dammann grating, see Fig. 6 (g, h). Their corresponding phases are shown in Fig. 6 (b, c), respectively. Although the topological charge of vortex phase in each channel can be adjusted freely, their orders remain the same. For this reason, we call these plasmonic focuses in Fig. 6 (g, h) as scalar plasmonic vortex. Their topological charges are shown in Fig. 6 (l, m), respectively.

Based on the principle of mode extraction, we convert the above scalar plasmonic vortices in Fig. 6(g, h) into their vector counterparts, namely 3 × 3 PVV modes with integer-order in Fig. 6(i) and fractional-order in Fig. 6(j). Here, Fig. 6 (d, e) are their corresponding phases of incident m = 30-order VVB, respectively. Their corresponding orders are denoted in Fig. 6(n, o). It should be emphasized that PVV with $l + 0.5$ order in Fig. 6 (j) is achieved with a stable $l + 0.5$ order VVB. According to Eq. (14), an optical vortex must adhere to the polarization of $l + 0.5$ order VVB mode so that its polarization state can maintain stably in free space, and PVV with fractional-order can be obtained on the gold film. That is, fractional-order PVV modes also possess an identical optical

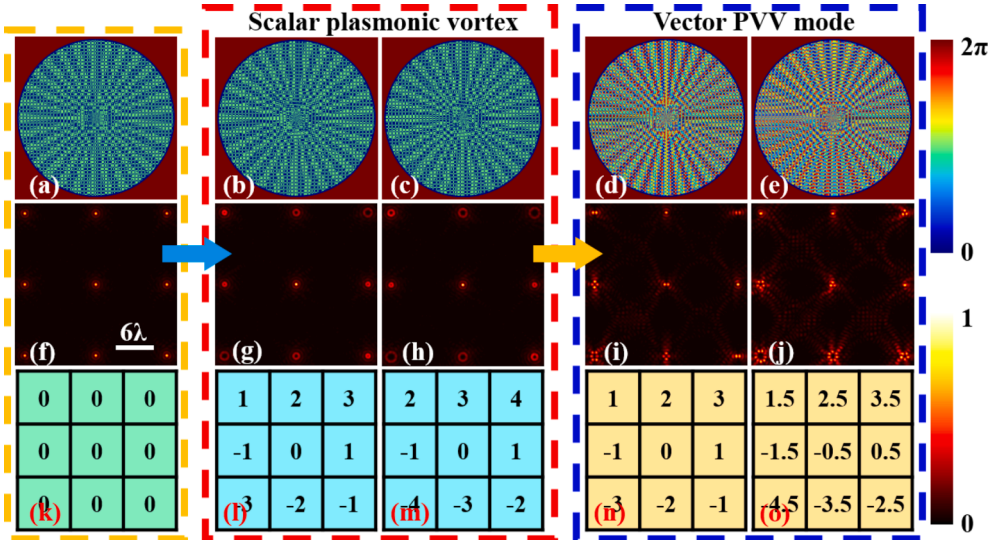

Fig. 6. PVV mode with 3 × 3 channels. Uniform 1-order PVV mode with 3 × 3 channels in (f) are created by the phase (a), which can be considered as the superposition of ϕ_i with $l = 1$ in Eq. (15) and a Dammann grating. (k) represents the topological charge of (f). By adjusting the parameter of Dammann grating realized by optical pen in Eq. (17), 3 × 3 scalar plasmonic vortices are obtained by the phases (b, c), the topological charges of which are shown in (l, m), respectively. Using the phases (d, e), both 3 × 3 scalar plasmonic vortices in (g, h) convert into 3 × 3 PVV modes with integer- and fractional-order in (i, j). Their corresponding orders are shown in (n, o), respectively.

vortex with + 0.5 topological charge in Fig. 6(j). Similar symmetry of topological charge in Fig. 6 (m) can therefore be realized by overlapping + 0.5 topological charge with the orders in Fig. 6 (o), which is the reason why we correspond the topological charge distribution in Fig. 6 (m) with that of Fig. 6(o). In addition, the total intensity of scalar plasmonic vortices in Fig. 6(g, h) created by Dammann grating is equal with that of uniform plasmonic focuses in Fig. 6 (f). As the topological charge increases, the energy density of scalar plasmonic vortex decreases. That is, the intensity of each scalar plasmonic vortex is different from each other because of the different topological charge. However, this disadvantage can be overcome by adjusting the parameter s_i of optical pen in Eq. (17). That is, with the aid of optical pen, one can not only adjust the polarization mode of PVV at will, but also the amplitude of each PVV modes individually, see Fig. 6 (i, j).

To further verify the versatility of multi-channel PVV modes, Fig. 7 presents multi-channel PVV modes with controllable shape. As shown in Fig. 7 (b, e), integer- and fractional-order PVV modes with the shape of square and "N" are generated by modulating the incident $m = 30$-order VVB with the phases in Fig. 7 (a, d). Their corresponding orders can be found in Fig. 7 (c, f), respectively. In Fig. 7 (c), the polarization mode of each PVV is adjusted by the parameter φ_0, where $\varphi_0 = 0.25\pi$ for point A, E; $\varphi_0 = 0.5\pi$ for point B, F; $\varphi_0 = 0.75\pi$ for point C, G; $\varphi_0 = \pi$ for point D, H. The topological charges of −0.5-order PVV modes are + 0.5 for point E, G (green box); −0.5 for point F, H (blue box), respectively. In Fig. 7 (f), $\varphi_0 = -0.25\pi$ for the PVV modes in the pink boxes, and $\varphi_0 = 0$ for the other modes. Due to the polarization rotation of $l + 0.5$-order VVB in free space, l + 0.5-order PVV possess an additional angle $\tau = \pm 0.25\pi$ in the center of SPPs excitation ring on the gold film [33]. In case of + 0.5 topological charge, $\tau = +0.25\pi$. In case of −0.5 topological charge, $\tau = -0.25\pi$. For example, the polarization mode of PVV with $l + 0.5$ order on the gold film can be obtained by $\varphi_E = \varphi_0 + \tau$, where $\varphi_E = 0.5\pi$ for point E and $\varphi_E = 0.25\pi$ for point F, see Fig. 7 (b).

4. Discussion

In the following, we would like to discuss the differences between our work and previous researches. Normally, multiple plasmonic focuses are created on the metal film by an incident vector beam modulated by a Dammann grating [29,30]. For example, multiple plasmonic bright focuses, namely 1-order PVV in this paper, can be created by focusing a radially polarized beam couple with a Dammann grating, while petal-like plasmonic focuses can be achieved by a linearly polarized beam, see Ref [30]. Here, the number and position of plasmonic focuses are controlled by the Dammann grating, and the polarization mode of each plasmonic focus is determined by the polarization state of incident vector beam. Therefore, all plasmonic focuses in the array possess an identical polarization property that relates to the polarization state of incident vector beam. So far, multiple PVV modes with different order have not been achieved yet in the research field of nanophotonics.

By contrast, our work conveys an important physical idea. That is, arbitrary inherent polarization modes within a light beam can be extracted directly using a particular phase based on the principle of mode extraction, as shown in Fig. 8. That is, without having to change the incident vector beam in Fig. 1, one can not only switch the inherent polarization mode of $m = 30$-order VVB at will, but also create multiple inherent polarization modes in free space with the aid of optical pen. Each inherent polarization mode can induce a PVV mode with a particular order and amplitude in a prescribed position on the gold film. In this way, multi-channel PVV modes with integer and fractional-order are realized accordingly, see Fig. 8. More importantly, the polarization and channel information of PVV mode in each channel can be adjusted individually in a real-time and dynamically, which is the most advantage of our work over that of the previous studies.

In conclusion, we have theoretically demonstrated dynamic control of multi-channel PVV modes with integer- and fractional-order using the principle of mode extraction along with optical pen. Based on the principle of mode extraction, inherent polarization mode of $m = 30$-order VVB can be extracted freely. PVV mode with adjustable integer- and fractional-order can therefore be switched at will by the SPPs excitation of inherent polarization mode on the gold film. More interestingly, the switch of single PVV mode can further be extended to the adjustment of multi-channel PVV modes with optical pen. That is, by merely adjusting the phase of incident $m = 30$-order VVB, the order of PVV mode can not only be adjusted at will, but also the number, position, amplitude and phase of each PVV channel are manipulated flexibly. This work demonstrates the simultaneous creation of multi-channel PVV modes with integer- and fractional-order on the gold film, which may find valuable applications in the research field of nanophotonics.

Funding

National Key R&D Program of China (2021YFF0502900); National

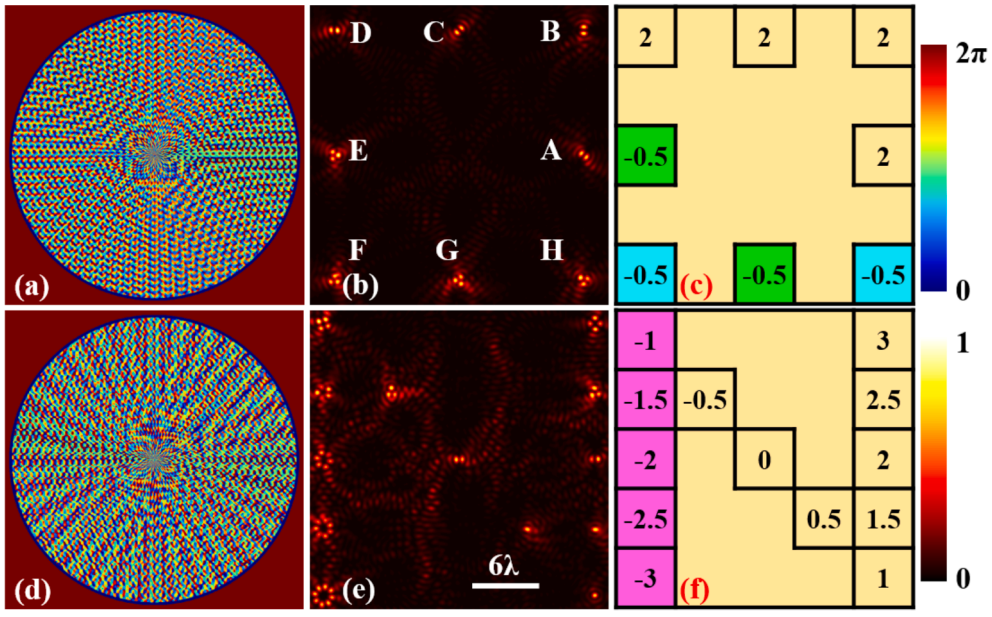

Fig. 7. Multi-channel PVV modes with controllable shape. Multi-channel PVV modes with the shape of square (b) and "N" (e) are generated by the phases in (a, d), respectively. Both orders of PVV modes are shown in (c, f), respectively. In subfigure (b), the polarization mode of each PVV is adjusted by the parameter φ_0, where $\varphi_0 = 0.25\pi$ for point A, E; $\varphi_0 = 0.5\pi$ for point B, F; $\varphi_0 = 0.75\pi$ for point C, G; $\varphi_0 = \pi$ for point D, H. The topological charges of −0.5-order PVV modes are + 0.5 for point E, G (green box); −0.5 for point F, H (blue box), respectively. In subfigure (f), $\varphi_0 = -0.25\pi$ for the PVV modes in the pink boxes, and $\varphi_0 = 0$ for the other modes. (For interpretation of the references to colour in this figure legend, the reader is referred to the web version of this article.)

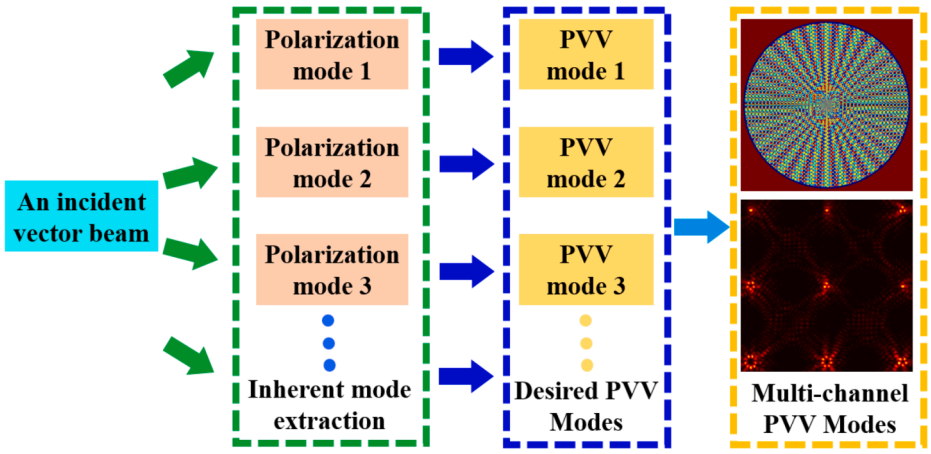

Fig. 8. Schematic entire process of dynamic control of multi-channel PVV modes. Using the principle of mode extraction along with optical pen, multiple inherent polarization modes can be extracted simultaneously from an incident vector beam, namely $m = 30$-order VVB in this paper. Multiple inherent polarization modes of incident vector beam can further induce multi-channel PVV modes with fractional- and integer-order on the gold film.

Natural Science Foundation of China (62022059/11804232/61835009/62127819); National Key Research and Development Program of China (2018YFC1313803); Shenzhen Key Laboratory of Photonics and Biophotonics (ZDSYS20210623092006020); Shenzhen Science and Technology Program (JCYJ20220818100202005).

Data availability

Data underlying the results presented in this paper are not publicly available at this time but may be obtained from the authors upon reasonable request.

CRediT authorship contribution statement

Yu Miao: Methodology, Writing – original draft. **Xiaoyu Weng:** Conceptualization, Methodology, Writing – review & editing. **Mingzhu Xu:** Visualization, Writing – review & editing. **Jun He:** Visualization, Writing – review & editing. **Liwei Liu:** Visualization, Writing – review & editing. **Changrui Liao:** Investigation, Validation. **Yiping Wang:** Investigation, Validation. **Xiumin Gao:** Writing – review & editing, Methodology, Validation, Supervision. **Baolin Liu:** Supervision, Project administration, Writing – review & editing. **Junle Qu:** Supervision, Project administration, Writing – review & editing. **Songlin Zhuang:** Supervision, Project administration, Writing – review & editing.

Declaration of Competing Interest

The authors declare that they have no known competing financial interests or personal relationships that could have appeared to influence the work reported in this paper.

Data availability

Data will be made available on request.

References

[1] G. Milione, M.P.J. Lavery, H. Huang, Y. Ren, G. Xie, T.A. Nguyen, E. Karimi, L. Marrucci, D.A. Nolan, R.R. Alfano, A.E. Willner, 4 x 20Gbit/s mode division multiplexing over free space using vector modes and a q-plate mode (de) multiplexer, Opt. Lett. 40 (9) (2015) 1980–1983.
[2] X. Weng, Y. Miao, G. Wang, Q. Zhan, X. Dong, J. Qu, X. Gao, S. Zhuang, Propagable optical vortices with natural noninteger orbital angular momentum in free space, Adv. Photonics Res. 4 (1) (2022) 2200094.
[3] K.S. Youngworth, T.G. Brown, Focusing of high numerical aperture cylindrical-vector beams, Opt. Express 7 (2) (2000) 77–87.
[4] H. Wang, L. Shi, B. Lukyanchuk, C. Sheppard, C.T. Chong, Creation of a needle of longitudinally polarized light in vacuum using binary optics, Nat. Photon 2 (8) (2008) 501–505.
[5] L. Fang, Z. Wan, A. Forbes, J. Wang, Vectorial Doppler metrology, Nat. Commun. 12 (1) (2021) 4186.
[6] B. Ndagano, I. Nape, M.A. Cox, C. Rosales-Guzman, A. Forbes, Creation and Detection of Vector Vortex Modes for Classical and Quantum Communication, J. Light. Technol. 36 (2) (2018) 292–301.
[7] D. Naidoo, F.S. Roux, A. Dudley, I. Litvin, B. Piccirillo, L. Marrucci, A. Forbes, Controlled generation of higher-order Poincaré sphere beams from a laser, Nat. Photonics 10 (2016) 327–332.
[8] G.M. Lerman, A. Yanai, U. Levy, Demonstration of nanofocusing by the use of plasmonic lens illuminated with radially polarized light, Nano Lett. 9 (5) (2009) 2139–2143.
[9] J. Sancho-Parramon, S. Bosch, Dark Modes and Fano Resonances in Plasmonic Clusters Excited by Cylindrical Vector Beams, ACS Nano 6 (9) (2012) 8415–8423.
[10] Z. Man, L. Du, C. Min, Y. Zhang, C. Zhang, S. Zhu, H.P. Urbach, X.-C. Yuan, Dynamic plasmonic beam shaping by vector beams with arbitrary locally linear polarization states, Appl. Phys. Lett. 105 (1) (2014), 011110.
[11] C. Min, Z. Shen, J. Shen, Y. Zhang, H. Fang, G. Yuan, L. Du, S. Zhu, T. Lei, X. Yuan, Focused plasmonic trapping of metallic particles, Nat. Commun. 4 (1) (2013) 2891.
[12] G. Spektor, E. Prinz, M. Hartelt, A.K. Mahro, M. Aeschlimann, M. Orenstein, Orbital angular momentum multiplication in plasmonic vortex cavities, Sci. Adv. 7 (33) (2021) eabg5571.
[13] Y. Zhang, J. Wang, J. Shen, Z. Man, W. Shi, C. Min, G. Yuan, S. Zhu, H.P. Urbach, X. Yuan, Plasmonic Hybridization Induced Trapping and Manipulation of a Single Au Nanowire on a Metallic Surface, Nano Lett. 14 (11) (2014) 6430–6436.
[14] T. Son, C. Lee, J. Seo, I.-H. Choi, D. Kim, Surface plasmon microscopy by spatial light switching for label-free imaging with enhanced resolution, Opt. Lett. 43 (4) (2018) 959–962.
[15] Z.D. Schultz, S.J. Stranick, I.W. Levin, Advantages and artifacts of higher order modes in nanoparticle-enhanced backscattering Raman imaging, Anal. Chem. 81 (23) (2009) 9657–9663.
[16] Y. Saito, P. Verma, Polarization-controlled Raman microscopy and nanoscopy, J. Phys. Chem. Lett. 3 (10) (2012) 1295–1300.
[17] S.A. Syubaev, A.Y. Zhizhchenko, D.V. Pavlov, S.O. Gurbatov, E.V. Pustovalov, A. P. Porfirev, S.N. Khonina, S.A. Kulinich, J.B.B. Rayappan, S.I. Kudryashov, A. A. Kuchmizhak, Plasmonic Nanolenses Produced by Cylindrical Vector Beam Printing for Sensing Applications, Sci. Rep. 9 (1) (2019) 19750.
[18] M. Liu, W. Zhang, F. Lu, T. Xue, X. Li, L. Zhang, D. Mao, L. Huang, F. Gao, T. Mei, J. Zhao, Plasmonic tip internally excited via an azimuthal vector beam for surface enhanced Raman spectroscopy, Photonics Res. 7 (5) (2019) 526–531.
[19] W.B. Chen, Q.W. Zhan, Realization of an evanescent Bessel beam via surface plasmon interference excited by a radially polarized beam, Opt. Lett. 34 (6) (2009) 722–724.
[20] C. Wu, S. Kumar, Y. Kan, D. Komisar, Z. Wang, S.I. Bozhevolnyi, F. Ding, Room-temperature on-chip orbital angular momentum single-photon sources, Sci. Adv. 8 (2) (2022) eabk3075.
[21] Y. Bai, J. Yan, H. Lv, Y. Yang, Plasmonic vortices: a review, J. Opt. 24 (8) (2022), 084004.
[22] A. Yang, L. Du, F. Meng, X. Yuan, Optical transverse spin coupling through a plasmonic nanoparticle for particle-identification and field-mapping, Nanoscale 10 (19) (2018) 9286–9291.
[23] Y. Dai, Z. Zhou, A. Ghosh, K. Kapoor, M. Dąbrowski, A. Kubo, C.-B. Huang, H. Petek, Ultrafast microscopy of a twisted plasmonic spin skyrmion, Appl. Phys. Rev. 9 (1) (2022), 011420.
[24] L. Huang, X. Chen, H. Mühlenbernd, G. Li, B. Bai, Q. Tan, G. Jin, T. Zentgraf, S. Zhang, Dispersionless Phase Discontinuities for Controlling Light Propagation, Nano Lett. 12 (11) (2012) 5750–5755.

[25] N. Yu, Z. Gaburro, Light Propagation with Phase Discontinuities: Generalized Laws of Reflection and Refraction, Science 334 (6054) (2011) 333–337.
[26] S. Wei, G. Si, M. Malek, S.K. Earl, L. Du, S.S. Kou, X. Yuan, J. Lin, Toward broadband, dynamic structuring of a complex plasmonic field, Sci. Adv. 4 (6) (2018) eaao0533.
[27] Z. Jin, D. Janoschka, J. Deng, L. Ge, P. Dreher, B. Frank, G. Hu, J. Ni, Y. Yang, J. Li, C. Yu, D. Lei, G. Li, S. Xiao, S. Mei, H. Giessen, F.M. Heringorf, C.W. Qiu, Phyllotaxis-inspired nanosieves with multiplexed orbital angular momentum, eLight 1 (2021) 1–11.
[28] H. Kano, S. Mizuguchi, S. Kawata, Excitation of surface-plasmon polaritons by a focused laser beam, J. Opt. Soc. Am. B 15 (4) (1998) 1381–1386.
[29] J. Bar-David, G.M. Lerman, L. Stern, N. Mazurski, U. Levy, Generation of a periodic array of radially polarized Plasmonic focal spots, Opt. Express 21 (3) (2013) 3746–3755.
[30] X. Weng, L. Wang, W. Yan, J. Qu, Tunable plasmonic focus array generated by Dammann grating in tightly focusing system, J. Opt. 21 (1) (2019), 015001.
[31] X. Weng, Q. Song, X. Li, X. Gao, H. Guo, J. Qu, S. Zhuang, Free-space creation of ultralong anti-diffracting beam with multiple energy oscillations adjusted using optical pen, Nat. Commun. 9 (1) (2018) 5035.
[32] X. Weng, Y. Miao, Q. Zhang, G. Wang, Y. Li, X. Gao, S. Zhuang, Extraction of inherent polarization modes from an m-Order vector vortex beam, Adv. Photonics Res. 3 (8) (2022) 2100194.
[33] X. Weng, Y. Miao, Y. Li, X. Dong, X. Gao, S. Zhuang, Physical essence of propagable fractional-strength optical vortices in free space. arXiv:2208.01929 [physics. optics] (2022).